World Conference on Timber Engineering Oslo 2023

NUMERICAL SIMULATION OF MOISTURE-INDUCED CRACKING IN INDOOR CLIMATE

Florian Brandstätter[1], Maximilian Autengruber[2], Markus Lukacevic[3], Josef Füssl[4]

ABSTRACT: Wood has the property to absorb and desorb moisture due to its hygroscopicity resulting in dimensional changes. Due to constrained non-uniform direction-depending expansion caused by moisture changes and gradients, respectively, stresses are induced, which may lead to crack initiation and propagation, reducing the load-bearing capacity of timber structures. However, little is known about the correlation between moisture changes or gradients and crack depths, and no quantitative prediction exists of crack depths caused by moisture gradients. Thus, based on numerical simulations, the cracking process for different initial moisture contents (MC) and various relative humidity (RH) reductions is investigated for two solid timber and one glued laminated timber cross-section. As a result, correlations between moisture gradients and maximum crack depths are derived, thus enabling the estimation of crack depths. The investigation revealed that cross-section size significantly influences the relation. In addition, more significant moisture gradients occur in larger cross-sections, resulting in earlier crack initiation compared to smaller ones, and crack development in larger cross-sections tends to last longer.

KEYWORDS: Extended finite element method, Multisurface failure criterion, Crack depth, Indoor climate, Wood

1 INTRODUCTION

Wood is a building material that is significantly affected by moisture. About 50% of the damages in timber constructions subjected to indoor climate conditions are caused by high and low moisture content (MC) as well as MC changes, with about half of the damage being cracks [1]. As wood is a hygroscopic material, the cell walls of wood absorb and desorb moisture from the surrounding climate, resulting in volume changes, which are additionally influenced by temperature. The strains caused by variations in MC and temperature induce stresses, as the non-uniform direction-dependent expansion is constrained. Increasing the stress level can lead to crack initiation and propagation if the strength of wood is exceeded, reducing the load-bearing capacity of timber structures. In addition, MC and temperature also influence material properties, such as strength and stiffness, which vary with the directions characteristic of wood (longitudinal, radial, and tangential). The effect of MC on material properties is limited by the so-called fiber saturation point (FSP) [2], which is the maximum amount of bound water in wooden cells. If further moisture is absorbed, it is present as free water in the lumen in addition to water vapor.

The most intense MC changes for indoor applications occur during the first winter after construction and from the beginning of erection until commissioning [1]. From December to February, the RH indoors can decrease to an average of 30 % [3-6] for two to four weeks resulting in an equilibrium MC of 8.2 % in case of pure desorption. Under uncommon conditions [7], even average RH levels of 25 % (7.2 % MC) over 30 days and 20 % RH (6.2 % MC) over 22.5 days occur. As the initial MC of wooden timber elements after production is usually between 10 % and 12 % [8], and DIN EN 14081-1:2019 allows measurement errors of ±3 % [9], during the first winter, immense moisture differences likely occur, inducing significant stresses, which may result in crack formation. However, it is unknown how deep moisture-induced cracks may propagate, and no quantitative relationship exists between crack depth and MC gradients caused by moisture changes.

Based on numerical simulations, this work aims to find a correlation between crack depth and moisture gradients and quantitatively estimate the crack depth in indoor climate conditions. Therefore, a moisture transport model based on the multi-Fickian theory [10-15] and a model for fracture in wood using the extended finite element method (XFEM) for the simulation of crack development are defined in Section 2. In addition, to find a relation for two solid timber (ST) and one glued laminated timber (GLT) cross-sections, numerous drying scenarios, which are characterized by different initial MCs and different drying loads, are simulated. When the simulation is initialized, the temperature is kept constant, but the initial RH is

[1] Florian Brandstätter, Vienna University of Technology (TU Wien), Austria, florian.brandstaetter@tuwien.ac.at
[2] Maximilian Autengruber, Vienna University of Technology (TU Wien), Austria, maxilian.autengruber@tuwien.ac.at
[3] Markus Lukacevic, Vienna University of Technology (TU Wien), Austria, markus.lukacevic@tuwien.ac.at
[4] Josef Füssl, Vienna University of Technology (TU Wien), Austria, josef.fuessl@tuwien.ac.at

https://doi.org/10.52202/069179-0054

decreased in a single step, which causes the moisture field to change and induce stresses. A multisurface failure criterion [16-19] is used to evaluate whether the induced stresses lead to crack formation. Section 3 illustrates the drying scenarios' results, and the relation between moisture gradient and crack depth is analyzed. In Section 4, the conclusion and outlook are shown.

2 MATERIALS AND METHODS

For the investigation of the relation and the prediction of the crack depth, two simulations per drying scenario are performed. In the first, moisture fields are determined based on the multi-Fickian theory. In the subsequent XFEM simulation, the moisture fields are used as a loading for the stress simulation based on linear-elastic material behavior (viscoelasticity, mechano-sorption, and plastification are not considered). For each increment in each integration point, stresses are calculated, and cracks initiate or propagate if they exceed the wood's strength. The latter is defined by a multisurface failure criterion presented in [16-19].

The commercial finite element software Abaqus (from Dassault Systèmes, Vélizy-Villacoublay, France) was used for the simulations. Quadratic brick elements with linear interpolation functions (C3D8) were used to discretize the cross-sections, and the equations were solved using the modified Newton method. The material is defined as cylindrical-orthotropic in each integration point to enable the consideration of different pith locations of the cross-sections.

2.1 MATHEMATICAL MODEL FOR MOISTURE TRANSPORT IN WOOD

The moisture transport model of [10-15] was used based on the multi-Fickian theory. It describes the transport of water vapor c_v in the lumen, as well as the transport of the bound water c_b in the cells, where the sorption rate $\dot{c}_{bv}$ is used to couple both processes, considering a hysteresis effect. As the MC in the simulations never exceeds the FSP, it is assumed that no free water occurs. To determine the change of the bound water, water vapor and energy, the following three differential equations are used:

Conservation of bound water concentration:

$$\frac{\partial c_b}{\partial t} = \frac{\partial}{\partial x} D_b \frac{\partial c_b}{\partial x} + \dot{c}_{bv} \tag{1}$$

Conservation of water vapor concentration:

$$\frac{\partial c_v}{\partial t} f_{lum} = \frac{\partial}{\partial x} D_v \frac{\partial c_v}{\partial x} f_{lum} - \dot{c}_{bv} \tag{2}$$

Conservation of energy:

$$\begin{aligned} \frac{\partial (ph)}{\partial t} = {} & \frac{\partial}{\partial x} K \frac{\partial T}{\partial x} + \frac{\partial}{\partial x} D_b \frac{\partial c_b}{\partial x} \overline{h}_b + \frac{\partial}{\partial x} D_{bT} \frac{\partial T}{\partial x} \overline{h}_b \\ & + \frac{\partial}{\partial x} D_v \frac{\partial c_v}{\partial x} h_v f_{lum} \\ & + \dot{c}_{bv} (h_v - h_b) \end{aligned} \tag{3}$$

On the left-hand side of Equations (1) to (3) the change rate of the concentrations c_b and c_v as well as of the energy (ph) are defined. The transport tensors of bound water D_b and water vapor D_v describe the diffusion processes, while K accounts for the thermal conduction. While c_b is related to the whole volume of the representative volume element (RVE), c_v is only referred to the volume proportion of the lumen f_{lum}. Whereas $\overline{h}_b$ and h_b define the average and specific enthalpy of bound water, respectively, h_v describes the enthalpy of water vapor.

The constitutive equations for the model are obtained from Autengruber et al. [20]. To implement equations (1) to (3) in Abaqus, the user element subroutine UEL was used.

[13] investigated the interaction between water vapor and bound water, using the sorption rate for description. An isothermal hysteresis was assumed for the simulations, as the temperature was kept constant.

For the initial conditions, it is assumed that the initial bound water concentration $c_{b,ini}$ and the initial water vapor concentration $c_{v,ini}$ are in equilibrium. $c_{b,ini}$ derives from the initial temperature T_{ini} and $c_{v,ini}$, which depends on the initial RH level.

The surrounding climate influences the moisture transport at the wood surfaces, where the effects are considered with Neuman boundary conditions. The given fluxes of water vapor Φ_v and energy Φ_T across the boundary are described by the following equations:

$$\Phi_v = k_{c_v}(c_v - c_{v,0}) f_{lum} \tag{4}$$

$$\Phi_T = k_T(\mathrm{T} - T_0) + k_{c_v}(c_v - c_{v,0}) f_{lum} h_v \tag{5}$$

with

$$k_{c_v} = \frac{Sh}{L} D_{air} \tag{6}$$

k_{c_v} is a film boundary coefficient that considers air flow and convection depending on air speed and surface roughness. Sh is 1 and L is 0.035 m [10] and $D_{air}$is the diffusion coefficient for water vapor in air. k_T defines the heat transfer coefficient and $T_0$is the temperature of distant air, where T is kept constant at 293.15 K.

2.2 MODEL FOR FRACTURE IN WOOD

After the moisture simulation, an XFEM simulation is performed to determine stresses caused by constrained shrinkage deformations, where the moisture fields are used as loading. For the XFEM simulations, moisture-dependent stiffness properties are presented, and the multisurface failure criterion from [16-19], defining the strength of wood, is introduced. The user element subroutine UDMINI was used to implement the criterion in Abaqus. In addition the enrichment regions for all cross-sections are defined and a certain distance is introduced, which is to be referred to as crack depth.

The moisture-dependant material properties of wood are based on the micromechanics material model of [21] with a clear wood dry density of 420 kg m^{-3} for Norway spruce (Picea abies). Based on this, elasticity tensor components for MC levels between 3 % and 30 % were determined and implemented in *Abaqus* (see [22] for details).

For the strength of wood, a multisurface failure criterion from [18], which considers the structure of wood at the

https://doi.org/10.52202/069179-0054

level of annual rings (late- and earlywood), is used. Based on multiple load combinations, the criterion was formulated, leading to eight Tsai-Wu surfaces [23] for the definition of failure:

$$f_i^{cw}(\sigma) = a_{LL,i}\sigma_{LL} + a_{RR,i}\sigma_{RR} + a_{TT,i}\sigma_{TT} + b_{LLLL,i}\sigma_{LL}^2 + b_{RRRR,i}\sigma_{RR}^2 + b_{TTTT,i}\sigma_{TT}^2 + 2b_{RRTT,i}\sigma_{RR}\sigma_{TT} + 4b_{LRLR,i}\tau_{LR}^2 + 4b_{RTRT,i}\tau_{RT}^2 + 4b_{TLTL,i}\tau_{TL}^2 \leq 1 \quad (7)$$

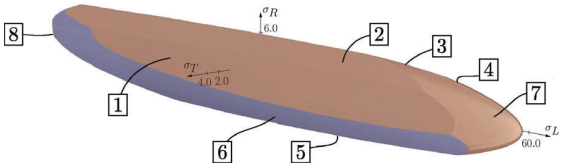

Figure 1: *Surfaces of the failure criterion, illustrated in the* $\boldsymbol{\sigma_{LL} - \sigma_{RR} - \sigma_{TT}}$ *stress space from [18].*

Only the surfaces describing brittle failure (surfaces 1,2,3, and 7) are considered in this work. If the induced stresses exceed the limits of the criterion, the corresponding failure surface defines the orientation of the crack initiation or propagation. The strength limits vary depending on the material orientation (longitudinal 56 MPa, radial 5 MPa, and tangential 2 MPa).

In *Abaqus*, so-called enrichment regions have to be defined to enable cracking. Unless multiple elements violate the failure criterion within the same time increment, only one crack can initiate per region. The enrichment configuration of the cross-sections is based on [22]. While for the GLT cross-section each lamella is divided into two equal-sized regions, one on top of the other, a cross-section configuration of eight rows and three columns is used for the ST cross-sections.

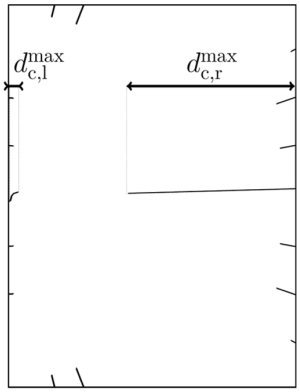

Figure 2: *Exemplary crack pattern of the cross-section ST 6 x 8. The deepest cracks on both the left and right edges are defined as* $\boldsymbol{d_{c,l}^{max}}$ *and* $\boldsymbol{d_{c,r}^{max}}$*, respectively.*

In the XFEM simulations, the crack pattern development is expected to vary depending on cross-section size, initial MC, and drying load. As the deepest cracks affect the safety of structures most, the maximum crack depth is analyzed to describe the evolution of the crack pattern, where the crack depth d_c is defined as the perpendicular distance from the surface to the crack tip. Since cracks on both edges are expected, the maximum crack depths on the left ($d_{c,l}^{max}$) and right ($d_{c,r}^{max}$) edges are determined and subsequently summed, defined as the maximum total crack depth d_c^{max} (see Figure 2).

2.3 DRYING SCENARIOS

Initially, the MC, which results from the surrounding RH, is uniform across the cross-section. When the simulation is initialized, the RH is reduced in a single step to a certain level, which is kept constant for 30 days, leading to moisture field changes. The RH level is reduced so that the expected equilibrium MC is decreased by a Δu_{equ} of 1 % up to 15 % (see Table), considering the desorption isotherm. Due to the non-linear shape of the isotherm, different initial MC levels (10.0 %, 11.9 %, 15.3 %, and 22.0 %) are investigated, which correspond to the RH levels 40.0 %, 50.0 %, 65.0 %, and 85.0 %, respectively. The initial values are based on RH, as this is easier to measure than Δu_{equ} in wood components. The initial RH values derive from the limits of the service classes in EC 5 [24].

Table 1: *Overview of the single-step relative humidity (RH) reductions at the boundary, resulting in differences in equilibrium moisture content* $\boldsymbol{\Delta u_{equ}}$ *of 1 % up to 15 % from four initial RH levels (40 %, 50 %, 65 %, and 85 %) determined with the desorption isotherm.*

Δu_{equ}	initial RH [%] (initial MC [%])			
	40 (10.0)	50 (11.9)	65 (15.3)	85 (22.0)
1	34.6	44.8	61.0	82.6
2	29.0	39.4	56.6	80.0
3	23.8	34.0	51.8	77.4
4	18.8	28.6	46.8	74.4
5	14.4	23.2	41.4	71.0
6	10.6	18.4	36.0	67.6
7	7.4	14.0	30.6	63.6
8	4.4	10.2	25.2	59.6
9	2.0	7.0	20.2	55.0
10	0.0	4.2	15.6	50.2
11	-	1.8	11.6	45.0
12	-	0.0	8.2	39.6
13	-	-	5.2	34.2
14	-	-	2.6	28.8
15	-	-	0.6	23.4

2.4 GEOMETRIES

For the simulations, two solid timber (ST) and one glued laminated timber (GLT) cross-section are studied in this work. The cross-sections are ST 6 x 8, ST 14 x 28, and GLT 20 x 40 (width x height in centimeters), commonly used for timber structures (see Figure 3). The pith location of the ST cross-sections is in the middle of the left edge,

as the deepest cracks are expected for this configuration, as shown by [22]. The lamella height of the GLT cross-section is 4 cm, the pith is located in the middle of the bottom, and the lamellas' orientation is based on common production standards [9]. It is assumed that the glue lines are made of melamine, which only minimally affects moisture transport since the diffusion characteristics of melamine and solid timber are similar [25].

To model plain-strain conditions, only one element with a depth of 1 mm in the longitudinal direction is defined. An overview of the other dimensions of the mesh is presented in Table 2. A hinged support in the center point and a roller support in the middle of the cross-section's right edge are defined for the geometric boundary conditions. Plain-strain conditions are assumed, and therefore, no deformations out-of-plane are allowed. In addition, no initial eigenstresses from, e.g., production processes, are assumed.

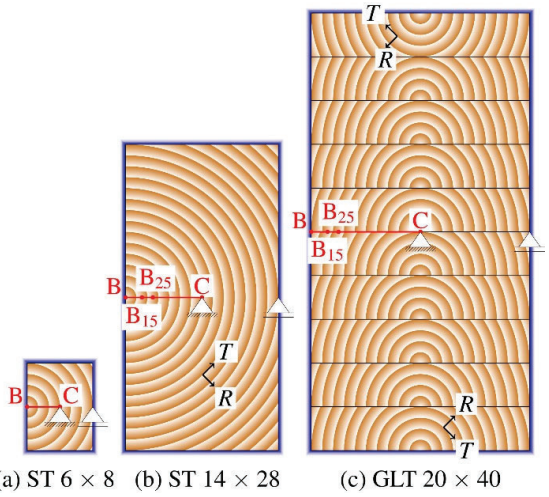

Figure 3: *Illustration of the used cross-sections, including the annual rings, pith locations, the definition of the local coordinate systems, and finite element node reference points: B, B_{15}, B_{25}, and C, where B_{15} and B_{25} are 15 mm and 25 mm, respectively, distant to the boundary. B_{15} and B_{25} are required for the moisture gradient definition in Section 3.2 [26].*

Table 2: *Mesh configurations of the cross-sections*

Elements	ST		GLT
	6 x 8	14 x 28	20 x40
Number	60 x 80	60 x 84	60 x 80
Width [mm]	1	2-4	2-5
Height [mm]	1	2-5	5

3 RESULTS

In the following, the crack initiation and propagation process is presented as well as the development of d_c^{max} for all initial MCs and Δu_{equ} are analyzed. The relationship between moisture gradients and crack depth is investigated based on the development results.

First, the crack initiation and propagation process are described in more detail using Figure 4, where the initial RH was reduced from 65 % to 20.2 % (final state) for the GLT 20 x 40 (see Figure 4 a). This results in a Δu_{equ} of 9 %. When the moisture simulation is initialized, the uniform moisture field adapts to the single-step reduction of the RH, leading to a non-uniform moisture distribution (see Figure 4 b). In the subsequent XFEM simulation, the stresses induced by the moisture field are determined per increment. At the same time, in each integration point, the multisurface failure criterion is evaluated, and if its limits are exceeded, cracks initiate (see Figure 4 c) or propagate (see Figure 4 d and e). Cracking is finished as soon as the criterion is not fulfilled anymore (see Figure 4 f).

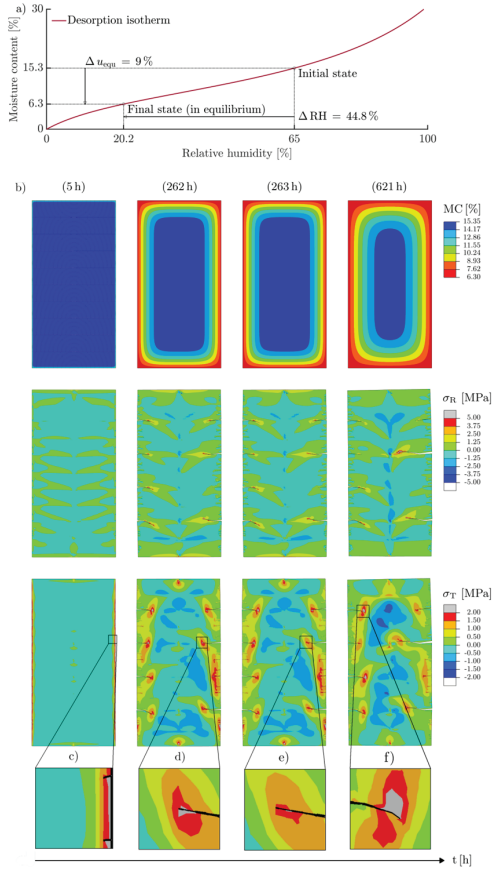

Figure 4: *Cracking process description: (a) Reducing the relative humidity causes moisture field adaptions (b). Stresses, such as $\boldsymbol{\sigma_R}$ and $\boldsymbol{\sigma_T}$, cause (c) initiation and (d-e) propagation of cracks, if the multisurface failure criterion is violated. As soon as the moisture-induced stresses no longer exceed the limits of the criterion, the cracking process is completed [26].*

3.1 CRACK DEPTH DEVELOPMENT

Before the crack depth development investigation, the crack formation at the end of the simulations for all cross-sections is presented, exemplified for an MC reduction from 15.3 % to 2.3 % (Δu_{equ} = 13 %) to show a characteristic crack pattern. For the ST cross-sections, multiple cracks on the top, bottom, and right edge occur,

https://doi.org/10.52202/069179-0054

whereas, on the left edge, only a few cracks can be seen due to the pith's location. However, it is noticeable that for the ST 6 x 8, the deepest crack is located at the middle height, while for the ST 14 x 28, the deepest one is at three quarters of the height. In the case of Δu_{equ} below 12 %, for the ST 14 x 28, the deepest crack also occurs in the middle of the cross-section. Furthermore, additional simulations confirmed that deep vertical cracks can be observed for the ST 14 x 28, which is related to the height-to-width ratio. The GLT 20 x 40 shows a different cracking behavior compared to the ST cross-sections. As the piths are located at the bottom of the lamellas, cracks occur on both the left and right edges. It can be seen that there are lamellas with one deeper and one shorter crack, as well as lamellas with three tiny cracks occur.

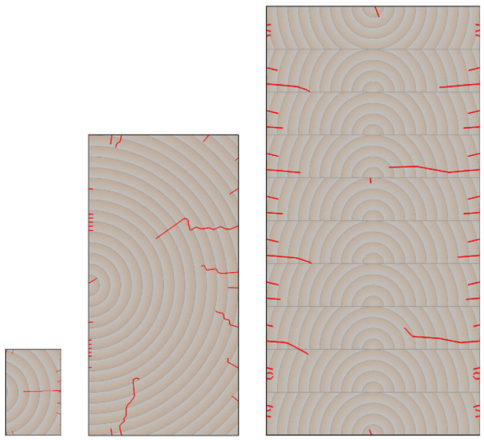

(a) ST 6 × 8 (b) ST 14 × 28 (c) GLT 20 × 40

***Figure 5**: Overview of the crack pattern for all cross-sections at the end of the simulation (t = 30 d), exemplified for a reduction of the initial MC from 15.3 % to 2.3 %. In addition, the pith location and the annual rings are illustrated. [26].*

In the following, the development of d_c^{max} is analyzed. Therefore, for all cross-sections, the evolution of d_c^{max} for different MCs and various Δu_{equ} over the complete simulation time is illustrated in Figure 6. For each drying scenario, $d_{c,l}^{max}$ and $d_{c,r}^{max}$ were documented at 0.25 d, 0.5 d, 1 d, 2 d, 3 d, 5 d, 10 d, 15 d, 20 d, 25 d, and 30 d, and subsequently, d_c^{max} was determined. [27] presented that $d_{c,l}^{max}$ and $d_{c,r}^{max}$ of 15 mm to 30 mm are in an acceptable range for timber structures to be considered safe, but the shape of the GLT girder, as well as the type of load, should be matched to the expected crack depth in the design of timber structures. Therefore, for the GLT cross-section in Figure 6, a d_c^{max} of 2 x 15 cm is marked. As the load-bearing capacity of ST cross-sections is also affected by cracking, a depth of 15 mm is highlighted because the pith location results in an asymmetric crack formation.

Figure 6 shows the development of d_c^{max} for all cross-sections under all drying scenarios given in Table 2, where d_c^{max} is given both in mm and in percent (cracked width). For all cross-sections, it can be seen that with increasing cross-section size, cracking stops later under the same conditions. For the ST 6 x 8, cracking ends between 1 d and 3 d, while for the GLT 20 x 40, crack propagation comes to a halt between 5 d and 30 d (in a few cases, the theoretical crack formation can even last longer than 30 d). This is related to the reduction of the MC in the cross-section's center. As soon as the RH is reduced, the MC decreases from both edges toward the center at the same rate. When the center is reached, the MC reduction is accelerated by the contribution of the opposite side. If the boundary condition is applied to only one side, the MC reduction rate would not be increased, as shown in [28]. Therefore, for smaller cross-sections, cracking stops earlier compared to larger cross-sections. In addition, it is noticeable that for the GLT 20 x 40 and the ST 14 x 28, cracking occurs from a Δu_{equ} of 3 %, whereas for the ST 6 x 8, a Δu_{equ} of 4 % is required for cracks to initiate. Only in the case of an initial MC of 22.0 %, a Δu_{equ} of 4 % leads to the first cracks for the ST 14 x 28. Since the moisture distribution is similar during the first hours and the MC in the center is minimally reduced, it can be concluded that cross-section size influences the drying load required to cause crack initiation due to larger moisture-induced stresses. The remaining effects on crack depth development caused by variation in Δu_{equ} are described in detail in [26].

3.2 RELATION OF CRACK DEPTH AND MOISTURE GRADIENT

Since a quantitative prediction of d_c^{max} seems possible for installations where equilibrium MC is given initially, the relation between crack depth and moisture gradient is studied. Dietsch et al. [1] revealed that about 50 % of the damages in timber structures are related to low and high MC and MC changes, resulting in moisture gradients. In [1], they were evaluated between 15 mm and 25 mm from the surface [28]. In this work, a similar approach was chosen: the moisture gradient is defined as the difference in MC between the two points P_1 and P_2, divided by their distance $(\Delta u/\Delta x)_{P_1P_2}$. [22] showed that the deepest moisture-induced cracks occurred when the difference in MC between the surface and the center was at maximum. It follows that the positions where the moisture gradient is evaluated also have to be considered. Therefore, the positions B, B_{15}, B_{25}, and C located on the path between B and C are investigated (see Figure 3), where B_{15} and B_{25} are 15 mm and 25 mm distant to the surface, respectively. For B_{15} and B_{25}, the nodes closest to them define the points for the moisture gradient, as at exactly 15 mm and 25 mm from the surface, there do not have to be finite element nodes (for details see [26]). The following three $(\Delta u/\Delta x)_{P_1P_2}$ configurations are examined: the moisture gradient between B and C $(\Delta u/\Delta x)_{BC}$, between B_{15} and B_{25} $(\Delta u/\Delta x)_{B_{15}B_{25}}$ and between B_{15}^B and B_{15}^c $(\Delta u/\Delta x)_{B_{15}^B B_{25}^C}$.

https://doi.org/10.52202/069179-0054

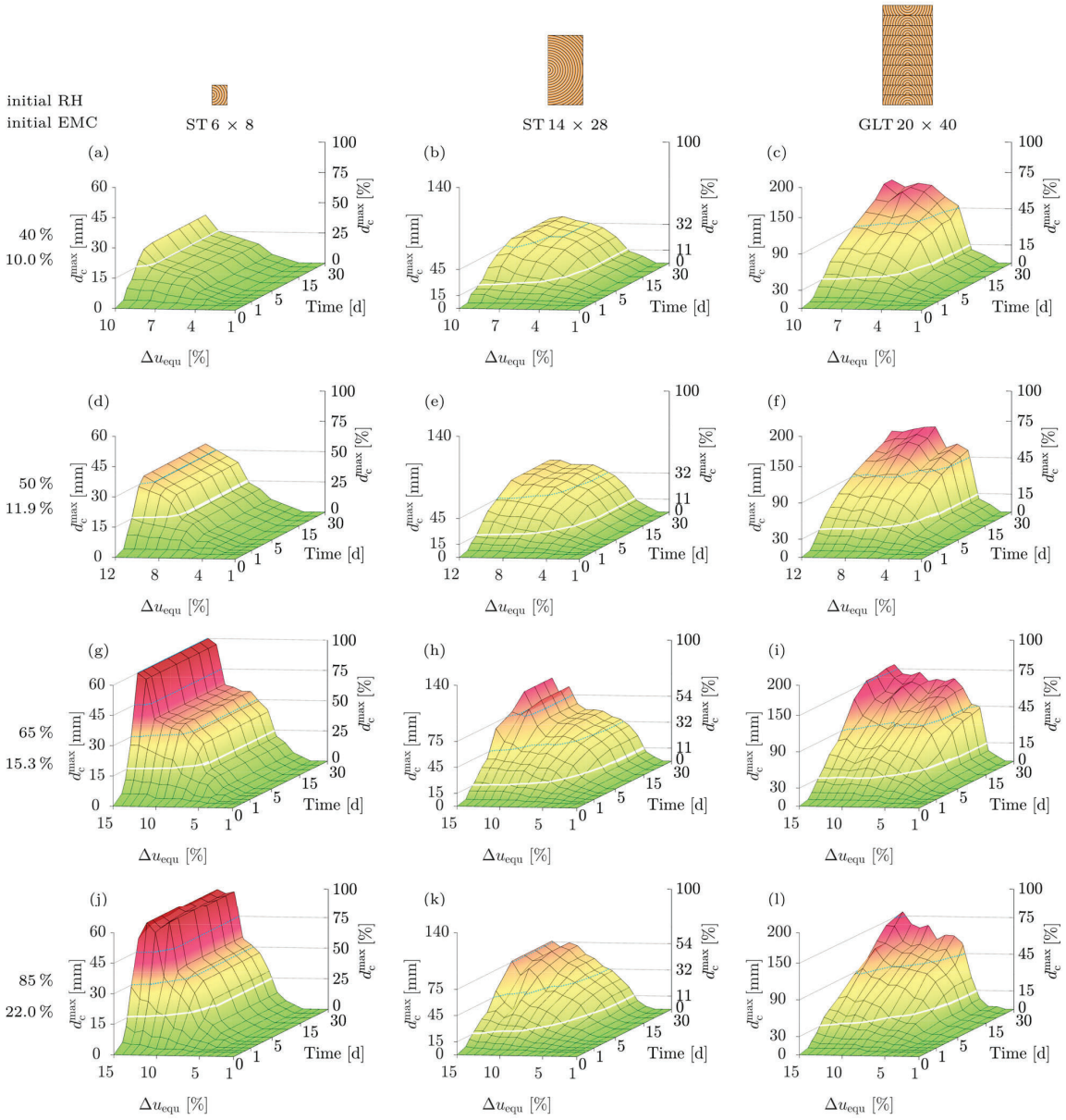

***Figure 6**: Development of the maximum total crack depth $\boldsymbol{d_c^{max}}$ (absolute and in percent of the width) for all cross-sections with initial moisture contents of 10.0 % (a, b and c), 11.9 % (d, e, and f), 15.3 % (g, h and i) and 22.0 % (j, k and l) when the equilibrium moisture content $\boldsymbol{\Delta u_{equ}}$ is reduced from 1 % up to 10 %, 12 % and 15 %, respectively, over 30 days. The white lines mark the limits (ST:15 mm; GLT: 30 mm), above witch the shape of the GLT girder as well as the type of load should be matched to the expected crack depth in the design of timber structures [27]. The blue dotted lines improve the perceptibility of $\boldsymbol{d_c^{max}}$ [26].*

In case of $(\Delta u/\Delta x)_{B_{15}^{B}B_{25}^{C}}$, the nodes closest to B15 are used for the definition of the moisture gradient, where one is closer to B (B_{15}^{B}) and the other closer to C (B_{15}^{C}). As the diffusion coefficients in radial and tangential directions are assumed equal, and the mesh is symmetrically along the vertical middle axis, B can be located on the left or on the right edge without affecting $(\Delta u/\Delta x)_{P_1P_2}$.

In the following, the approach to describe the relation between d_c^{max} and, exemplary, $(\Delta u/\Delta x)_{BC}$ is shown, with the result illustrated in Figure 7. For the ST 6 x 8, the developments of d_c^{max} and $(\Delta u/\Delta x)_{BC}$ are displayed with an initial MC of 15.3 % and for a Δu_{equ} of 5 %, 7 %, and 9 % (see Figure 7a). Observing Figure 7a reveals that for each point in time, a d_c^{max} can be connected to a $(\Delta u/\Delta x)_{BC}$, but as the deepest cracks are essential for the design of timber structures, the maximum d_c^{max} is related to the largest $(\Delta u/\Delta x)_{BC}$. More details about the relation and developments of Δu_{equ} and $(\Delta u/\Delta x)_{BC}$ are presented in detail in [26].

https://doi.org/10.52202/069179-0054

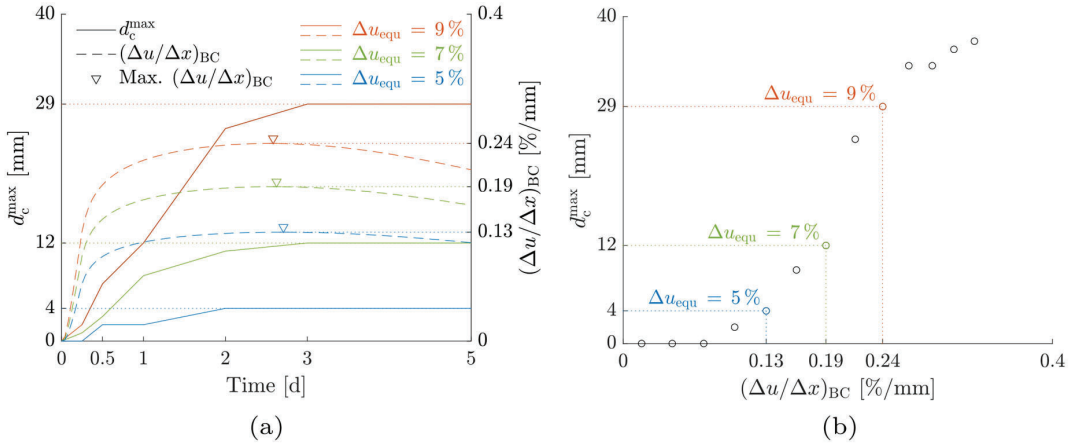

***Figure** 7: Relation between the moisture gradient $(\Delta u/\Delta x)_{BC}$ between the two points B and C (B: boundary; C: centre; see* Figure 3*) and the maximum total crack depth (d_c^{max}) for the ST 6 x 8with an exemplary initial moisture content of 15.3 % In (a), the developments of d_c^{max} and $(\Delta u/\Delta x)_{BC}$. for three different reductions of the equilibrium moisture content Δu_{equ} (*5 %, 7 % and 9 %*) are displayed. In (b), the maxima of d_c^{max} and $(\Delta u/\Delta x)_{BC}$. For Δu_{equ} reductions from 1 % up to 13 % are shown, illustrating the relation between d_c^{max} and $(\Delta u/\Delta x)_{BC}$ [26].*

In Figure 7 b), the maxima of d_c^{max} and $(\Delta u/\Delta x)_{BC}$. For Δu_{equ} reductions from 1 % up to 13 % are shown, excluding 14 % and 15 %, as they are assumed outliers. Observing the data, an exponential increase can be seen, followed by a leveling off of the trend. This behavior can be described with the so-called Gompertz function, which is defined as:

$$d_c^{max}((\Delta u/\Delta x)_{P_1P_2}) = g^{max} e^{-g^l e^{-g^g (\Delta u/\Delta x)_{P_1P_2}}} \quad (8)$$

with d_c^{max} as the maximum total crack depth in mm, the moisture gradient between two points, P1 and P2, $(\Delta u/\Delta x)_{P_1P_2}$ in [%/mm] as well as the function parameters g^{max}, g^{l}, and g^{g}. g^{max} defines the asymptote and, therefore, the maximum d_c^{max}, g^{l} sets the displacement along the ordinate axis, and g^{g} describes the inflection point's growth rate.

Next, the influence of the moisture gradient configuration on the relation is investigated (see Figure *8*). For all cross-sections, the relation between d_c^{max} and $(\Delta u/\Delta x)_{BC}$, $(\Delta u/\Delta x)_{B_{15}B_{25}}$, and $(\Delta u/\Delta x)_{B_{15}^{B}B_{25}^{C}}$ with an initial MC of 15.3 % is illustrated, where for each configuration, the best fitting Gompertz function and the corresponding coefficient of determination are shown. As the coefficients of determination are all above 0.97 and the curves fit the data, it follows that such functions can be used to relate the moisture gradients to d_c^{max}, depending on the size of the cross-section. The differences between the configurations are minimal, and therefore, for further investigations, $(\Delta u/\Delta x)_{BC}$ is recommended, due to better possible prediction of the MC at the boundary and the center for larger cross-sections, as presented by [29]. More details about the influence of the moisture gradient configurations on the relation are presented in [26]. In addition, in [26], the effect of varying initial MC on the relation is investigated, and the influence of reducing the RH linearly over time on crack depth development is studied. Furthermore, a simplified crack depth determination for indoor climate conditions is presented.

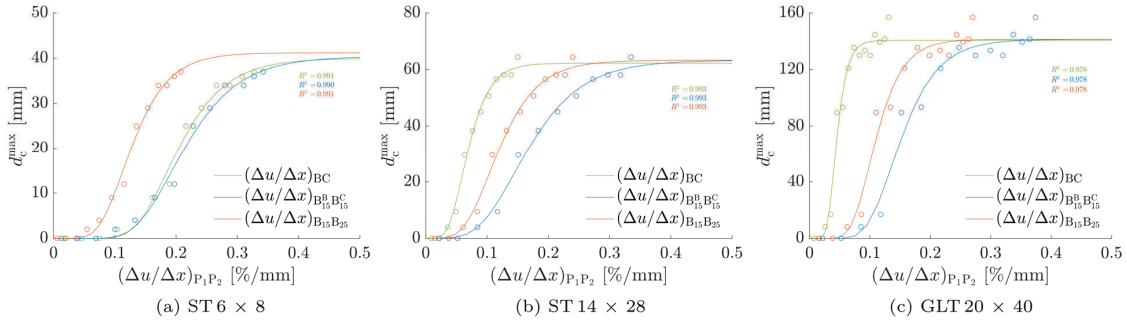

***Figure** 8: Development of the maximum total crack depth d_c^{max} depending on the moisture gradient configuration between two points P_1 and P_2 $(\Delta u/\Delta x)_{P_1P_2}$ to analyse the effect of the positions P_1 and P_2 (B, B_{15}, B_{25}, and C) on the relation with an initial MC of 15.3 % for all cross-sections. The positions are on the path between boundary B and center C (see* Figure 3*). The data illustrated as circles represent the maxima of d_c^{max} related to the maxima of the corresponding $(\Delta u/\Delta x)_{P_1P_2}$ (see Figure 7) [26].*

https://doi.org/10.52202/069179-0054

4 CONCLUSIONS AND OUTLOOK

To quantitatively estimate crack depths in indoor climate conditions and to find a relation between crack depth and moisture gradient, in this work, the crack depth development of two solid timber and one glued laminated timber cross-section for different immediate RH reductions and initial MCs was analyzed numerically. Based on the simulation results, a relation between the maximum total crack depth d_c^{max}, which is the sum of the deepest cracks on the right and left side, and the moisture gradient was established. Thus, the prediction of d_c^{max} in indoor climate conditions for installations, where after production, timber members are protected from environmental influences to have a uniform initial moisture field at the beginning of the operation, seems possible. A multi-Fickian moisture transport model [10-15] was used to simulate the moisture distribution developments within the cross-sections. Those were then used as a loading for the subsequent XFEM simulations, where moisture-induced stresses were determined considering linear-elastic material behavior. For these fracture simulations, a multisurface failure criterion [18] for describing failure behavior and a multiscale material model [21] to determine the moisture-dependant stiffness tensor were used. The main findings are summarised as follows:

- Moisture gradients were correlated to d_c^{max}, where the relation depends on cross-section size.
- In larger cross-sections, larger moisture gradients occurred, which is why cracks initiate earlier compared to smaller cross-sections.
- For larger cross-sections, crack propagation lasted longer than for smaller cross-sections.

For future work, the cracking behavior of different cross-sections or wood products could be analyzed. E.g., [30] used these models to investigate the moisture transport in a timber-concrete composite plate after cast-in-place concrete application, indicating potential moisture-induced cracking behavior due to low surrounding RH.

ACKNOWLEDGEMENT

The funding from the Austrian Science Fund (FWF) through the START project Y1093 "Virtual Wood Labs", the SFB F77 "Advanced Computational Design", and the Forest Value project InnoCrossLam are gratefully acknowledged.

REFERENCES

[1] P. Dietsch, A. Gamper, M. Merk, S. Winter, Monitoring building climate and timber moisture gradient in large-span timber structures, *Journal of Civil Structural Health Monitoring*, 5 (2): 153–165, 2015.

[2] J. Siau: Transport Processes in Wood, Springer-Verlag Berlin Heidelberg, New, York Tokyo, 1984

[3] J. Ferdyn-Grygierek, Indoor environment quality in the museum building and its effect on heating and cooling demand, *Energy and Buildings*, 85: 32-44, 2014.

[4] J. L. Nguyen, J. Schwartz, D. W. Dockery, The relationship between indoor and outdoor temperature, apparent temperature, relative humidity, and absolute humidity, *Indoor Air*, 24 (1): 103–112, 2014.

[5] S. Hameury, T. Lundström, Contribution of indoor exposed massive wood to a good indoor climate: in situ measurement campaign, *Energy and Buildings*, 36 (3): 281–292, 2004.

[6] T. Log, Indoor relative humidity as a fire risk indicator, *Building and Environment*, 111: 238 – 248, 2017.

[7] T. Alsmo, C. Alsmo, Ventilation and relative humidity in swedish buildings, *Journal of Environmental Protection*, 5: 1022 – 1036, 2014.

[8] P. Dietsch, Effect of reinforcement on shrinkage stresses in timber members, *Construction and Building Materials*, 150: 903–915, 2017.

[9] DIN EN 14081-1:2019 10 01: Timber structures – Strength graded structural timber with rectangular cross-section – Part 1: General requirements (Berlin: Deutsches Institut für Normung, 2019).

[10] J. Eitelberger, K. Hofstetter, S. Dvinskikh, A multiscale approach for simulation of transient moisture transport processes in wood below the fiber saturation point. *Compos. Sci. Technol*., 71 (15): 1727–1738, 2011

[11] S. Fortino, A. Genoese, A. Genoese, L. Nunes, P. Palma, Numerical modelling of the hygro-thermal response of timber bridges during their service life: A monitoring case-study. *Constr. Build. Mater*. 47: 1225–1234, 2013

[12] S. Fortino, P. Hradil, G. Metelli, Moisture-induced stresses in large glulam beams. case study: Vihantasalmi bridge. *Wood Material Science & Engineering*, 14 (5): 366–380, 2019

[13] H.L. Frandsen, L. Damkilde, S. Svensson, A revised multi-Fickian moisture transport model to describe non-Fickian effects in wood. *Holzforschung*, 61: 563-572, 2007.

[14] D. Konopka, M. Kaliske, Transient multi-fickian hygro-mechanical analysis of wood. *Computers Struct*., 197: 12–27, 2018

[15] K. Krabbenhoft, L. Damkild: A model for non-fickian moisture transfer in wood, *Materials and Structures*, 37(9): 615–622, 2004.

[16] M. Lukacevic, J. Füssl, R. Lampert: Failure mechanisms of clear wood identified at wood cell level by an approach based on the extended finite element method, *Engineering Fracture Mechanics*, 144:158–175, 2015.

[17] M. Lukacevic, J. Füssl, Application of a multisurface discrete crack model for clear wood taking into account the inherent microstructural characteristics of wood cells. *Holzforschung*, 70 (9): 845–853, 2016

[18] M. Lukacevic, W. Lederer, J. Füssl: A microstructure-based multisurface failure criterion for the description of brittle and ductile failure mechanisms of clear-wood, *Engineering Fracture Mechanics*, 176:83–99, 2017.

https://doi.org/10.52202/069179-0054

[19] M. Li, J. Füssl, M. Lukacevic, J. Eberhardsteiner, C. M. Martin, Strength predictions of clear wood at multiple scales using numerical limit analysis approaches. *Computers & Struct*. 196 200–216, 2018
[20] M. Autengruber, M. Lukacevic, J. Füssl, Finite-element-based moisture transport model for wood including free water above the fiber saturation point. *Int. J. Heat Mass Tran*. 161 (Nov. 2020) 120228.
[21] K. Hofstetter, C. Hellmich, J. Eberhardsteiner, Development and experimental validation of a continuum micromechanics model for the elasticity of wood, European Journal of Mechanics - A/Solids 24 (6) 1030–1053. 2005
[22] M. Autengruber, M. Lukacevic, C. Gröstlinger, J. Füssl. Finite-element-based prediction of moisture-induced crack patterns for cross-sections of solid wood and glued laminated timber exposed to a realistic climate condition. Constr. Build.Mater.;271:121775, 2021
[23] Tsai SW, Wu EM. A general theory of strength for anisotropic materials. *J Compos Mater.* 5(1):58–80, 1971
[24] Austrian Standards International, ÖNORM B 1995-1-1:2019-06-01. Eurocode 5: Design of timber structures – Part 1-1: General – Common rules and rules for buildings – Consolidated version with national specifications national comments and national supplements for the implementation of ÖNORM EN 1995-1-1 (Vienna: Austrian Standards, 2019).
[25] T. Volkmer, J.-A. Schmidt, K. Kranitz, P. Niemz, Untersuchungen zum Einfluss der Klebstoffart auf den Diffusionswidertand von Holzverklebungen, Bauphysik 34 (2) 55–60. 2012
[26] F. Brandstätter, M. Autengruber, M. Lukacevic, J. Füssl. Prediction of moisture-induced cracks in wooden cross-sections using finite element simulations (in revision)
[27] P. Frech, Beurteilungskriterien für rissbildung im konstruktiven holzbau, Fraunhofer IRB Verlag (1998)
[28] S. Svensson, G. Turk, T. Hozjan, Predicting moisture state of timber members in a continuously varying climate, Engineering Structures 33 (11) 3064–3070. 2011
[29] M. Autengruber, M. Lukacevic, C. Gröstlinger, J. Eberhardsteiner, J. Füssl, Numerical assessment of wood moisture content-based assignments to service classes in EC5 and a prediction concept for moisture-induced stresses solely using relative humidity data, Engineering Structures 245 112849. 2021
[30] M. Lukacevic, M. Autengruber, T. Raimer, J. Eberhardsteiner, J. Füssl, Effect of cast-in-place concrete application on moisture distribution in timber-concrete composite floors with notched connections, investigated via finite element simulations, Journal of Building Engineering 42 103005. 2021